Experimental and theoretical study of the electronic structure of $PtGa_2$

Li-Shing Hsu
Department of Physics, National Chang-Hua University of Education, Chang-Hua 50058, Taiwan, Republic of China

G. Y. Guo
Department of Physics, National Taiwan University, Taipei 106, Taiwan, Republic of China
and Synchrotron Radiation Research Center, Hsinchu 300, Taiwan 106, Republic of China

J. D. Denlinger and J. W. Allen
Randall Laboratory, University of Michigan, Ann Arbor, Michigan 48109-1120

(Received 31 May 2000; revised manuscript received 5 September 2000; published 26 March 2001)

Synchrotron-radiation-excited angle-resolved photoemission and x-ray-absorption spectra for the (111) face of $PtGa_2$ are presented, along with derived experimental dispersion relations. These bands are compared with those obtained from a theoretical band-structure calculation. The x-ray-absorption near-edge spectra agree with the calculated site- and symmetry-decomposed partial density-of-states curves, and electrons transfer from Pt to Ga in forming the $PtGa_2$ compound. Extended x-ray-absorption fine-structure spectra of $PtGa_2$ are analyzed to yield its structural parameters. The energy variation of the Pt $5d$ bands for $PtGa_2$ shows atomiclike behavior in the photon energy range of 80 to 220 eV.

DOI: 10.1103/PhysRevB.63.155105 PACS number(s): 79.60.−i

I. INTRODUCTION

Binary intermetallic compounds that crystallize in the cubic fluorite (CaF_2) structure have received a great deal of attention owing to their many unique properties. It is interesting to note that these intermetallics exhibit a striking variety of colors, ranging from purple ($AuAl_2$) to copper ($PtIn_2$) to gold ($PtAl_2, PtGa_2$). Many of these phases also become superconducting at low temperatures.[1,2] Moreover, such compounds are excellent systems for studying the transition-metal $5d$ bands, since group-III elements contribute only *s-p* states to the valence band (VB). One example is the study of the positions of the Au 5d bands for $AuAl_2$,[3] $AuGa_2$,[4] and $AuIn_2$.[3,4] Over the past 12 years, the electronic structure of another interesting compound, $PtGa_2$, has been studied by performing band-structure calculations,[5,6] optical-absorption[6] and Raman scattering[7] studies, x-ray and uv photoemission spectroscopic (XPS and UPS) experiments,[5] and synchrotron-radiation-excited angle-integrated photoemission measurement.[8] The gold color of $PtGa_2$ was explained in terms of its Au-like density of states (DOS) and the less than 10% difference of the binding energies (E_B) of the three Γ points (Γ_8^1, Γ_7, and Γ_8^2) between this material and Au. The electronic structures and many physical properties of AuX_2 ($X=$Al, Ga, or In) and $PtGa_2$ (Refs. 2 and 9) have been reported and reviewed.[10] Even though an angle-resolved photoemission spectroscopic (ARPES) study of $AuGa_2$ and $AuIn_2$ was published long ago,[4] no such work on $AuAl_2$ and $PtGa_2$ has been reported so far.

There are two published relativistic band-structure calculations for $PtGa_2$: one was done by using the mixed-basis band-structure interpolation scheme (MBBSIS),[5] the other was performed by using the linear augmented-plane-wave (LAPW) method with the muffin-tin potential approximation.[6] The former treated the crystal-field and spin-orbit (SO) interactions as adjustable fitting parameters to the XPS or UPS spectra, while the latter included SO interaction as a perturbation. It is noted that the total DOS calculated by these two methods showed three Pt $5d$ bands (Γ_8^1, Γ_7, and Γ_8^2), and all these bands were resolved in a high-resolution angle-integrated photoemission spectroscopic (PES) study.[8] The focus of this paper will be on mapping the bands of $PtGa_2$ along Γ-L, using normal-emission ARPES data from the (111) face of a $PtGa_2$ single-crystal sample. Furthermore, these bands are compared with those obtained from the full-potential relativistic band-structure calculation. Another intention of this paper is to measure the x-ray-absorption near-edge spectra (XANES) of $PtGa_2$ and to compare it with the calculated site- and symmetry-resolved DOS curves. Extended x-ray-absorption fine-structure (EXAFS) spectra of $PtGa_2$ are also analyzed to yield its bonding parameters. Lastly, we use the tunability of synchrotron radiation to study the amplitude-modulation effect of the Pt $5d$ bands in this material. Preliminary results of part of this work have been published.[11]

This paper is organized as follows. In Sec. II the experimental and theoretical methods are described. In Sec. III the results and discussion are presented. The conclusions of this work are contained in Sec. IV.

II. METHODS

A. Experimental methods

Procedures for preparation of the (111) face of a $PtGa_2$ single crystal[12] were reported in previous papers.[5,8] The bulk sample contains $(34.3\pm0.1)\%$ Pt atoms.[12] ARPES experiments were performed at the undulator beamline 7.0 at the Advanced Light Source. Photon energies in the range of 80 to 220 eV were selected with a spherical-grating monochromator, and a Physical Electronics 137 mm hemispherical analyzer was used in the fixed-analyzer-transmission mode to collect the photoelectron spectra. With 150 lines/mm for grating setting and 3 eV for analyzer pass-energy setting, the

energy resolution was less than 80 meV. The angular resolution was less than $\pm 1°$, which corresponds to a momentum resolution of roughly 0.2 $Å^{-1}$ at 125 eV kinetic energy. The analysis chamber was also equipped with a low-energy electron-diffraction (LEED) system and a dual-anode Mg/Al x-ray source for XPS and x-ray photoelectron diffraction (XPD) measurements. The chamber pressure during the experiments was 2×10^{-10} Torr.

The sample surface was cleaned by repeated cycles of sputtering with Ar ions and annealing to 500 °C until photoemission spectra showed no traces of O or C contamination on the sample surface. The observed XPD and LEED patterns[11] further confirmed the cleanliness and ordering of the sample surface. The $PtGa_2$ surface after cyclic cleaning contained about 8% fewer Ga atoms than those in the bulk as determined from the area ratio of the Pt $5d$ and Ga $3d$ XPS peaks and the theoretical cross sections.[13] The preferential sputtering of the Ga atoms from the $PtGa_2$ surface agrees with observations made on surfaces of Ni_3Al,[14–16] Ni_3Ga,[15–18] NiGa,[16–19] and CoGa (Ref. 20) for Al or Ga deficiency after alternating cycles of Ar-ion bombardment and subsequent annealing. Study of the $AuGa_2$ (001) surface[21] by Auger electron spectroscopy and LEED showed that it is primarily Ga terminated and the Ga deficiency improves with annealing cycles.

X-ray-absorption (XAS) spectra for $PtGa_2$ were taken on wiggler beamline 17 C at the Synchrotron Radiation Research Center (SRRC), Taiwan. A Si(111) double-crystal monochromator was used and the typical energy resolution was about 2 eV. The XAS spectra were measured in total-electron-yield mode at the Pt L_3 edge and the Ga K edge of $PtGa_2$ at room temperature. Four scans were collected and averaged to increase the signal-to-noise ratio. Standard 4-μm-thick Pt foil was used as reference for energy calibration. Data at the Ga K edge were internally calibrated by setting the inflection point to 10 367.0 eV. The beam path was flooded with He to reduce the intensity attenuation of the low-energy x rays by air. The photon flux was obtained simultaneously by measuring the current of a Au mesh located near the exit slit of the monochromator and used for normalization of the XAS spectra. Analysis of the EXAFS spectra was carried out by using the UWXAFS 3.0 software package.[22] First, the EXAFS oscillation $\chi(E)$ in energy space of Pt foil and $PtGa_2$ was extracted from the measured absorption coefficient $\mu(E)$ by subtracting an isolated atomiclike background absorption function $\mu_0(E)$, using the relation $\chi(E)=[\mu(E)-\mu_0(E)]/\mu_0(E)$. Subsequently, $\chi(E)$ was converted into a k-space function, $\chi(k)$. Here k is the wave number of the ejected photoelectron given by $k=2\pi[2m_e(E-E_0)/h^2]^{1/2}$, where m_e is the mass of the electron. A typical form of the EXAFS function for a set of atoms at a particular distance is given by

$$\chi(k)=\sum_j N_j k^{-1} R_j^{-2} S_i^2 F_j(k)\exp(-2\sigma_j^2 k^2) \times \exp[-2R_j/\lambda_j(k)]\sin[2kR_j+\delta_{ij}(k)], \quad (1)$$

where $F_j(k)$ is the backscattering amplitude of the jth shell, S_i^2 the amplitude reduction factor, $\lambda_j(k)$ the mean free path of the photoelectron, and $\delta_{ij}(k)$ the total phase shift experienced by the photoelectron. The remaining terms in Eq. (1) include N_j, the coordination number of the jth shell, R_j, the mean distance between the absorber and the jth shell, and σ_j^2, the scaling constant in the Debye-Waller factor. These terms contain quantitative structural information, and can be obtained by curve-fitting analysis. Curve-fitting procedures began with the *ab initio* calculation of the phase-shift and amplitude functions for single scattering of atom pairs using the FEFF6 program.[23] The fitting was made in r space within the range of the specific peak. For a good fit, the goodness-of-fit parameter[23] was always below 0.02.

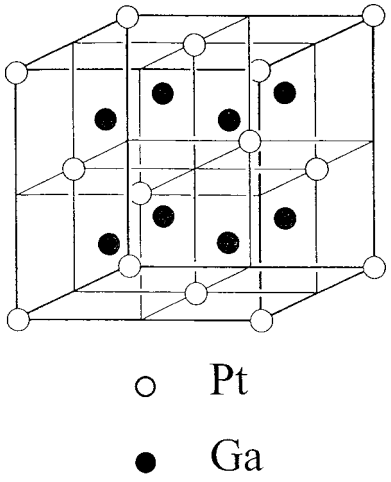

FIG. 1. Crystal structure of $PtGa_2$.

B. Theoretical methods

It is well known that the relativistic effects are large in AuX_2 (X=Al, Ga, or In) and in $PtGa_2$.[5,24] To interpret the ARPES data, we have calculated the relativistic band structure of $PtGa_2$ with the CaF_2 structure (shown in Fig. 1) and at the experimental lattice constant of 5.91 Å. We used the highly accurate all-electron full-potential linear augmented-plane-wave (FLAPW) method.[25] The calculations are based on the first-principles density-functional theory with the standard local-density approximation (LDA) to the exchange-correlation potential.[26] The muffin-tin radii used for the Pt and Ga atoms of $PtGa_2$ are 1.27 Å. The shallow $5p$ and $4f$ core states of Pt and the $3d$ states of Ga were also treated as band states by using the so-called local orbitals.[25] The wave functions, the charge densities, and the potentials were expanded in terms of the spherical harmonics inside the muffin-tin spheres. The cutoff angular momentum ($l_{\max}$) was 10 for the wave functions and 6 for the charge densities and the potentials. The Brillouin zone (BZ) integration was carried out using the improved tetrahedron method.[27] The number of augmented plane waves included was about 120 per atom, i.e., $R_{\mathrm{MT}}K_{\max}=9$.[25] The number of k points in the irreducible BZ wedge (IBZW) used in the self-consistent calculations was 72. To calculate the DOS curves and the theoretical XANES spectra, 165 k points in the IBZW were used. We have checked the convergence of the calculated eigenvalues with respect to the number of augmented plane

TABLE I. The theoretical and experimental lattice constant (a) and bulk modulus (B) of $PtGa_2$ and Pt metal. Both LDA and GGA scalar-relativistic calculations with and without spin-orbit (SO) coupling are listed for comparison.

Material	Method	a (Å)	B (Mbar)
$PtGa_2$	LDA	5.87	1.46
	LDA+SO	5.90	1.39
	GGA	6.03	1.08
	GGA+SO	6.08	1.00
	Expt.	5.91[a]	
Pt metal	LDA	3.89	3.31
	LDA+SO	3.92	2.55
	GGA	3.98	2.71
	GGA+SO	4.01	2.56
	Expt.	3.92[b]	2.4[c]

[a]E. Zintl, A. Harder, and W. Haucke, Z. Phys. Chem. Abt. B **35**, 354 (1937).

[b]*American Institute of Physics Handbook*, edited by D. E. Gray (McGraw-Hill, New York, 1972).

[c]*Metals Handbook*, 8th ed., edited by T. Lyman (American Society of Metals, OH, 1964).

waves and k points used. In particular, we found that increasing $R_{MT}K_{max}$ to 10 changed the relative positions of the eigenvalues at the Γ points by up to a few meV only.

Density-functional theory with the LDA has been used for first-principles studies of the physical properties of a variety of materials and provides an accurate theoretical estimate of static structural properties, crystal stability, and pressure-induced phase transformations in many solids.[28] Nonetheless, there are problems with the LDA. Notably, it predicted a wrong ground state for iron[29] and much too small lattice constants for $3d$ transition metals.[30] Therefore, the so-called generalized gradient approximation (GGA) corrections to the LDA have been developed in recent years.[31] These GGA calculations have been found to considerably improve the LDA results for $3d$ transition metals and other solids.[29,30,32] However, the GGA calculations do not give an improvement over the LDA for materials such as $5d$ transition metals for which the LDA already works rather well.[30] In the present paper, we have performed total-energy calculations for several lattice constants for $PtGa_2$ and Pt metal with and without the GGA. We derived the theoretical lattice constants and bulk moduli from these calculated total energies. They are shown in the third and fourth columns, respectively, in Table I. Clearly, the lattice constant calculated with the LDA plus SO coupling is in very good agreement with experiments for both $PtGa_2$ and Pt metal, and the GGA lattice constants are too large by up to 3% compared with experiments. Thus, we use the LDA rather than the GGA in the rest of this paper.

From Table I, there are some discernible relativistic (SO coupling) effects on the structural properties for $PtGa_2$. These relativistic effects reduce the difference between the calculated and measured lattice constant and bulk modulus. However, the most important relativistic effect is the splitting of the Γ_{25} states into Γ_7 and Γ_8 states, as will be discussed in the next section. We are not aware of any measurement of the bulk modulus for $PtGa_2$, although the elastic constants for $AuGa_2$ were measured by Testardi[33] and showed temperature dependence. Interestingly, the theoretical bulk modulus of $PtGa_2$ is quite close to that (1.12 Mbar) estimated earlier by Hsu[2] and that (0.96 Mbar) measured by Testardi[33] for $AuGa_2$. We have also performed spin-polarized calculations for $PtGa_2$ but no stable magnetic states could be found. This is consistent with the low DOS at the Fermi energy (E_F), as will be shown in the next section. Note that the DOS at E_F for $PtGa_2$ is much smaller than that for Pt metal, which is also not magnetic.

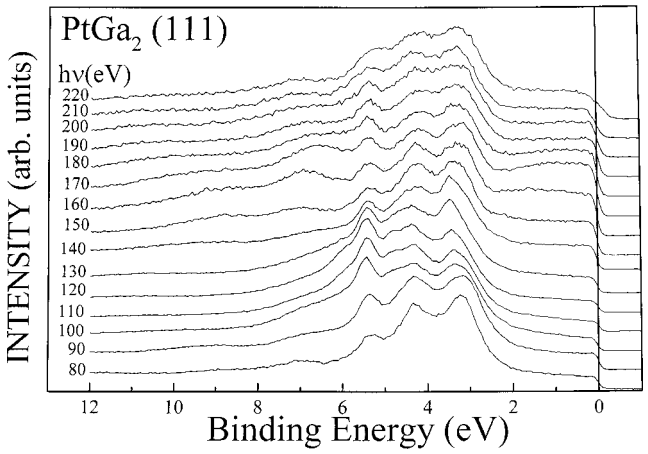

FIG. 2. Angle-resolved photoemission spectra taken at normal emission from the (111) face of $PtGa_2$ in the photon energy range 80 to 220 eV.

III. RESULTS AND DISCUSSION

A. Angle-resolved photoemission spectra and band structure

Figure 2 shows a set of normal-emission VB photoemission spectra from the (111) face of $PtGa_2$. The normal to the sample surface was determined from the Pt $4f_{7/2}$ XPD polar and azimuth scans.[11] The photon energy ($h\nu$) was varied from 80 to 220 eV so as to probe the fourth to the fifth BZ's. The E_F for $PtGa_2$ was assigned at half height on the onset of a plateau in Fig. 2. Using a direct-transition model and assuming a free-electron conduction-band structure, we plotted the energy versus momentum dispersion relation for $PtGa_2$ along L-Γ-L. It is displayed in Fig. 3 as open circles. The inner potential for $PtGa_2$ needed for determining the BZ position is estimated to be 12.3 eV. This value was taken to be the difference between the muffin-tin zero of energy (7.7 eV) in the FLAPW calculation and the vacuum level as determined from the work function of $PtGa_2$. Here we use the work function of $AuGa_2$ [4.63 eV (Ref. 4)] for $PtGa_2$. The shallow (<2 eV) and deep (>7 eV) s-p bands for $PtGa_2$ were determined not from the energy distribution curves but from the enhanced intensity maps. Two of these maps were published previously.[11] The same method was applied to the Pt $5d$ bands of $PtGa_2$ to double-check their positions. One should note here that surface disorder and phonons may make the band mapping for $PtGa_2$ at room temperature and the photon energies used less accurate. The band structure of

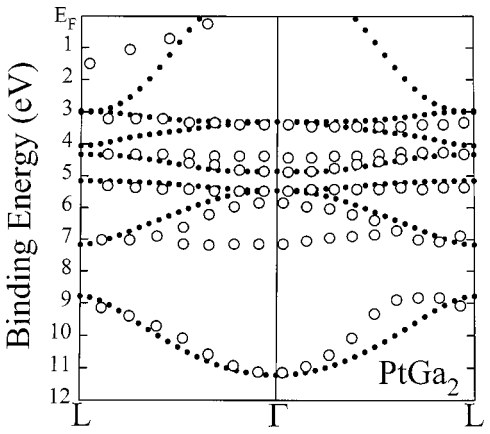

FIG. 3. Band structure of $PtGa_2$ along L-Γ-L. Open circles are bands derived from the ARPES data. Closed circles are theoretical band structure calculated by the FLAPW method.

$PtGa_2$ calculated by the FLAPW method, along with its Brillouin zone, is shown in Fig. 4. The band structure along Λ is also plotted as closed circles in Fig. 3 to compare with the experimentally determined bands. We first note that the flat Δ_2 band along Γ-X that appeared in the APW (Ref. 34) and LAPW (Ref. 6) band structures for $AuGa_2$ and in the MBBSIS band structures for $AuGa_2$ (Ref. 22) and $PtGa_2$ (Ref. 5) disperses more strongly across E_F in Fig. 4. The behavior of this Δ_2 band for $PtGa_2$ agrees with that obtained from the LAPW band structure[6] of $PtGa_2$ and with that derived from a thermoelectric power measurement[9] on $PtGa_2$. The Δ_2 band for $PtGa_2$ also shows similar dispersion to that for $AuAl_2$ and for $AuIn_2$.[22,34] This explains why the physical properties of $PtGa_2$ show no anomaly,[2,9] while quite a few physical properties of $AuGa_2$ are anomalous in the sense that they are significantly different from those of $AuAl_2$ and $AuIn_2$.[10] One of these anomalies is the temperature-dependent elastic constants of $AuGa_2$ mentioned in Sec. II B. The plateau in Fig. 2, which is caused by photoemission from the Pt s-p band (band 7), extends from E_F to $E_B = 2$ eV with fairly low intensity except for $h\nu$ between 160 and 190 eV, at which a higher-intensity but broader peak starts to move from $E_B = 1.5$ eV toward E_F. In general, s-p bands disperse much more rapidly than the almost flat d bands, thus accounting for the broader feature seen in the photoemission spectra. At $h\nu \geq 160$ eV, more final states are accessible for the Pt s-p states, which causes the higher intensity observed in the spectra. The Fermi-edge intensity maps[11] for $PtGa_2$ at $h\nu = 105$ eV (near the Γ point) clearly showed three bright rings centered at the L point in the second BZ. These rings originate from bands converging toward the L point and hence can be described as hole pockets. A polar-photon Fermi-edge intensity map[11] further showed that these rings do not close in the k_z direction and hence the Fermi surface for $PtGa_2$ is not a closed ellipsoid.

In Fig. 2, a three-peak structure with much higher intensity at higher E_B is due to the Pt $5d$ states. The E_B's of these peaks change by less than 0.3 eV on varying $h\nu$. Since dispersion of the Pt $5d$ bands in $PtGa_2$ is less than 0.3 eV along Λ in the BZ, the use of DOS peaks as band emissions from the Γ points in our previous angle-integrated photoemission

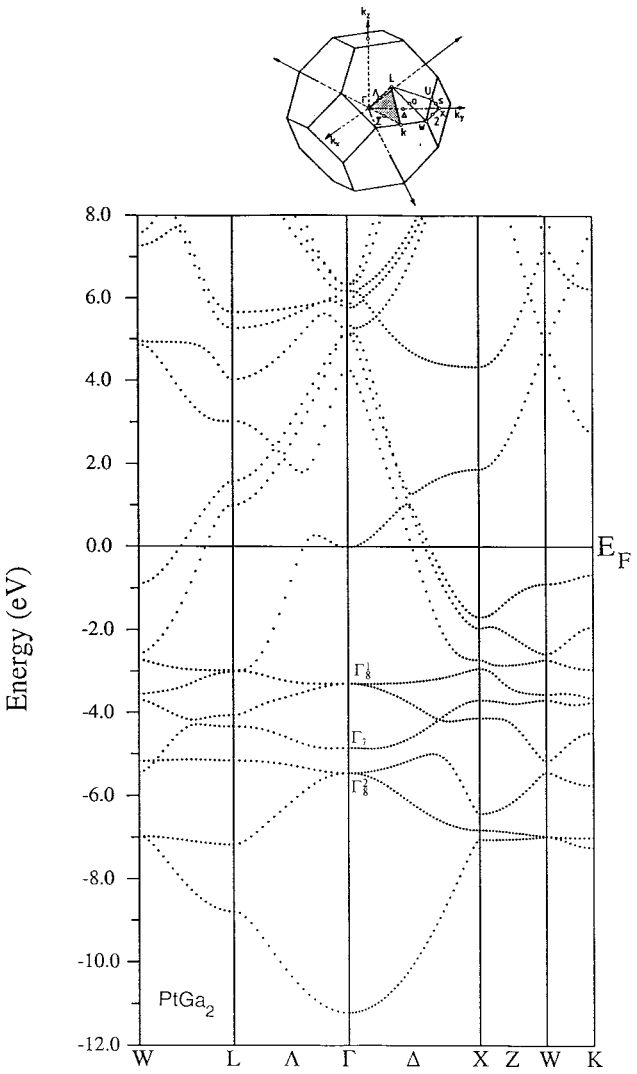

FIG. 4. Band structure of $PtGa_2$ calculated by the FLAPW method. Also shown is the Brillouin zone for $PtGa_2$.

work[8] is justified. The peak around $E_B = 7$ eV is due to emissions from the one-dimensional DOS.[35] It is identified as such because it resonates strongly at $h\nu = 160$ and 170 eV, at which energies the BZ boundary is reached; and is rather weak between $h\nu = 110$ and 130 eV, at which energies the center of the BZ is covered. The experimental band at $E_B = 4.7$ eV for $h\nu = 100$–130 eV involves a surface state, which was also observed from the (100) surfaces of $AuGa_2$ and $AuIn_2$.[4] This surface state was checked by exposing the sample surface to oxygen and observing its gradual disappearance.

The E_B values at Γ_8^1, Γ_7, and Γ_8^2 for Au and $PtGa_2$ obtained from photoemission measurements and band-structure calculations are listed in Table II. Three observations found in Table II should be pointed out here. First, the three E_B values at the Γ points for $PtGa_2$ obtained from this study and angle-integrated PES work[8] are essentially the same (within the energy resolution of 0.2 eV of the latter experiment). This result implies that the Pt $5d$ states in $PtGa_2$ are highly localized. Thus, the crystal-field ($10Dq$) and spin-orbit (ξ) parameters obtained from the present ARPES data ($10Dq$

TABLE II. The experimental and theoretical binding energies (E_B) of the Au and Pt $5d$ states at Γ for Au and $PtGa_2$, respectively. All values in eV.

$E_B(\Gamma_8^1)$	$E_B(\Gamma_7)$	$E_B(\Gamma_8^2)$	Method
	Au		
3.55	4.45	5.90	angle-resolved PES[a]
3.38	4.33	5.75	LRC[b]
3.29	4.34	5.65	APW[c]
3.09	4.34	5.52	FLAPW[d]
	$PtGa_2$		
3.40	4.40	5.47	angle-resolved PES[d]
3.55	4.20	5.35	angle-integrated PES[e]
2.79	3.71	4.86	MBBSIS[f]
3.80	4.84	5.52	LAPW[g]
3.34	4.88	5.45	FLAPW[d]

[a]Reference 38.
[b]Linear rigorous cellular method, Ref. 36.
[c]Augmented-plane-wave method, Ref. 37.
[d]Full-potential linear augmented-plane-wave method. This work.
[e]Reference 8.
[f]Mixed-basis band-structure interpolation scheme method, Ref. 5.
[g]Linear augmented-plane-wave method, Ref. 6.

$=0.9$ eV, $\xi=0.56$ eV) are the same as those obtained from angle-integrated PES data.[8] Secondly, the three $E_B(\Gamma)$ values for $PtGa_2$ obtained from the MBBSIS calculation[5] are lower by 0.6–0.7 eV than those obtained from the ARPES data. This means that, although the MBBSIS calculation generally preserves the relative positions of the Pt $5d$ bands in $PtGa_2$, an offset of about 0.65 eV should be added to the theoretical E_B values of the Pt $5d$ bands in order for them to be in agreement with those derived from the experimental data. We note that the $E_B(\Gamma_8^1)$ and $E_B(\Gamma_7)$ values obtained from the LAPW calculation[6] are larger by about 0.4 eV than the corresponding values obtained from the ARPES data; while the $E_B(\Gamma_8^2)$ values obtained from the LAPW calculation and the ARPES data are essentially the same. Disagreement for the $E_B(\Gamma_8^1)$ and $E_B(\Gamma_7)$ values between the LAPW calculation[6] and the ARPES data[4] was also found in $AuGa_2$. This means that, although the lower two transition-metal $5d$ bands are correctly calculated in the LAPW method, the upper three transition-metal $5d$ bands are roughly 10–12% larger in E_B than the ARPES data. This is probably due to the muffin-tin potential approximation used in the LAPW calculation. The best agreement among the $E_B(\Gamma)$ values for $PtGa_2$ was found between the present FLAPW calculation and the ARPES data, though the theoretical $E_B(\Gamma_8^1)$ value is still about 11% larger than the experimental value. We speculate that this disagreement may be inherent for the LDA used in the band-structure calculation.[24] Thirdly, our experimental $E_B(\Gamma)$ values for $PtGa_2$ are close to those for Au (3.55, 4.45, and 5.90 eV, respectively, in Table II). It seems that the combined crystal-field and SO effects cause the Pt $5d$ bands of $PtGa_2$ to be situated at positions within 8% of the Au $5d$ bands for Au metal. Therefore, this study reconfirms the similarity between the electronic structures of $PtGa_2$ and Au. It should also be pointed out that, in Table II, the $E_B(\Gamma)$ values for Au obtained from previous[36,37] and the present theoretical calculations are close to those obtained from the ARPES study.[38]

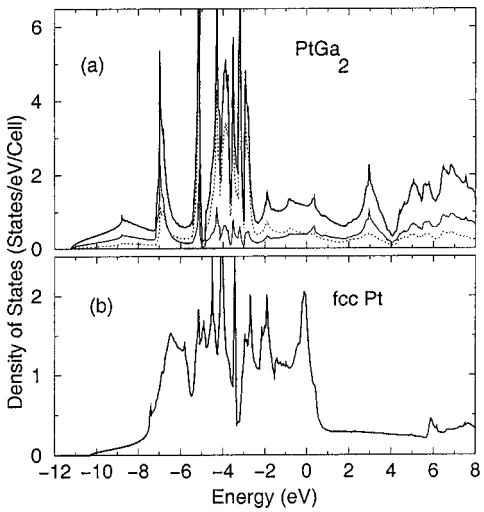

FIG. 5. (a) Total and site-decomposed densities of states for $PtGa_2$, and (b) total density of states for Pt metal calculated by the FLAPW method. In (a), the dotted line denotes the Pt site-decomposed density of states and the thin solid line that for Ga.

B. DOS curves and experimental and theoretical XANES spectra

The total DOS curves for $PtGa_2$ and for fcc Pt metal are shown as the solid lines in Figs. 5(a) and 5(b), respectively. Also shown in Fig. 5(a) are the Pt (dotted line) and the Ga (thin solid line) site-decomposed partial DOS's for $PtGa_2$. The energy zeros are the Fermi energies of the respective materials. The lattice constant and the muffin-tin radius used for Pt metal are 3.92 and 1.38 Å, respectively. The DOS at $E_F[n(E_F)]$ for $PtGa_2$ is 1.15 states/eV cell, which is comparable to that calculated by using the MBBSIS method (1.09 states/eV cell).[5] The $n(E_F)$ value obtained from a specific-heat measurement[2] (1.67 states/eV cell) is this ''band-structure'' DOS enhanced by a factor $1+\lambda$, where λ is the electron-phonon mass enhancement parameter. The λ value thus determined for $PtGa_2$ is 0.45. We note that this λ value is within 8% of the value (0.49) calculated by Hsu[2] using McMillan's formula[39] with a critical temperature of 2.15 K and a Debye temperature of 220 K for $PtGa_2$.

Figures 6(a) and 6(b) show, respectively, the experimental (solid line) and theoretical (dashed line) Pt L_3-edge XANES spectra for $PtGa_2$ and for Pt foil, while Fig. 6(c) shows the experimental (solid line) and theoretical (dashed line) Ga K-edge XANES spectra for $PtGa_2$. All the experimental spectra were divided by the incident photon intensity and then normalized to an edge jump of unity. The theoretical XANES spectra have been broadened with a Lorentzian of full width at half maximum of 4 eV to simulate the core-hole lifetime. From the relative peak positions in Figs. 6(a) and 6(b), one can immediately see that charge transfers from Pt to Ga in forming the compound $PtGa_2$. The Pt L_3 white-line

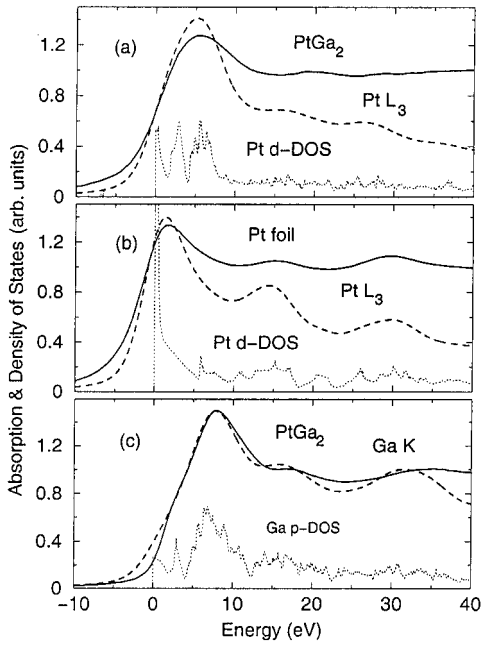

FIG. 6. Experimental (solid lines) and theoretical (dashed lines) spectra near (a) Pt L_3 edge for $PtGa_2$, (b) Pt L_3 edge for Pt metal, and (c) Ga K edge for $PtGa_2$. Also shown are (a) Pt d DOS for $PtGa_2$, (b) Pt d DOS for Pt metal, and (c) Ga p DOS for $PtGa_2$.

energy for $PtGa_2$ is shifted to a higher value relative to that for Pt foil. This energy shift is caused partly by the decreased effective nuclear charge which, in turn, is caused by an increase in the screening of the nucleus by the valence electrons. This edge shift may also be caused by variation of the composition of the nearest-neighbor shell of Pt atoms in $PtGa_2$. Quantitative analysis of the charge transfer in $PtGa_2$ will be discussed below. According to the dipole-transition selection rule, the Pt L_3 and Ga K white-line features correspond, respectively, to the transitions from Pt $2p_{3/2}$ to $5d_{5/2}$ and from Ga $1s$ to $2p$ states. Thus, also plotted in Fig. 6 are the relevant angular-momentum-decomposed partial DOS curves (dotted lines): Fig. 6(a) Pt d DOS for $PtGa_2$, Fig. 6(b) Pt d DOS for Pt metal, and Fig. 6(c) Ga p DOS for $PtGa_2$. The energy zeros are the energies of the inflection points for the Pt L_3 (11 564 eV) or Ga K (10 367 eV) absorption edges. Since the Pt L_3 white-line intensity is proportional to the density of unoccupied Pt $5d$ states, the larger area under the Pt L_3 white line for $PtGa_2$ than for Pt foil suggests that the total number of electrons at the Pt site for $PtGa_2$ is smaller than that for elemental Pt. This observation agrees with that obtained from the theoretical calculation presented below. We also notice that the agreement is rather good between the theoretical calculations and the XANES data for the peak positions. For example, the energies (with respective to the energies of the inflection points) of the peaks of the Pt L_3-edge and Ga K-edge experimental XANES spectra for $PtGa_2$ are 5.8 and 19.6 eV and 8.0, 16.7, and 35 eV, respectively; while the corresponding theoretical values are 5.3 and 15.3 eV and 7.8, 15.8, and 31.6 eV. For the peak heights, however, we note that the theoretical amplitudes of the Pt L_3 spectra in Figs. 6(a) and 6(b) become smaller and smaller compared with the corresponding experimental ones as the energy is increased. This decrease in peak height is due to the finite-sized, linearized energy-dependent basis sets in the muffin-tin spheres used in the present calculations. For example, only Pt $6s$, $5p$, $6p$, $5d$, and $4f$ orbitals are included inside the Pt muffin-tin spheres, which are sufficient to describe well the valence and low-lying conduction bands as well as near-edge XAS spectra. It would be necessary to include, e.g., Pt $6d$ and $7d$ orbitals to give a better high-energy Pt L_3 XAS spectrum. However, this latter approach is not our main concern in the present paper.

TABLE III. Total integrated number of electrons per atom for the valence orbitals at the Pt sites for Pt metal and for $PtGa_2$, and at the Ga site for $PtGa_2$.

	n_s	n_p	n_d	n_f	n_{total}
Pt site (Pt metal)	0.76	0.85	8.20	0.19	10.0
Pt site ($PtGa_2$)	0.46	0.51	8.12	0.25	9.34
Ga site ($PtGa_2$)	1.48	1.69	0.16		3.33

Listed in Table III are the total integrated number of electrons per atom for the valence orbitals at the Pt sites for Pt metal and for $PtGa_2$, and at the Ga site for $PtGa_2$. One should note that it is difficult to quantify the charge transfer from FLAPW band-structure calculations. This is because there is no unique way to assign the charge distribution in the interstitial region (i.e., outside the muffin-tin spheres) to individual atoms in the solid. We have therefore performed relativistic electronic-structure calculations for fcc Pt metal and for $PtGa_2$ using the linear muffin-tin orbital method with the atomic-sphere approximation.[40] In this method, there is no interstitial region and thus it is possible to estimate charge transfer. The same atomic radius of Pt was used for both fcc Pt metal and Pt in $PtGa_2$. The atomic radius of Pt (1.53 Å) was determined from the experimental unit-cell volume of fcc Pt metal. The atomic radius of Ga (1.63 Å) in $PtGa_2$ was determined from the experimental unit-cell volume of $PtGa_2$ minus the atomic volume of Pt. From these calculated numbers, one concludes that the total charge transfer from Pt to Ga when forming the $PtGa_2$ compound is roughly 0.7 electrons per atom, and that loss of the s, p, and d charges at the Pt site is observed. One also notes that the total number of valence electrons for $PtGa_2$ is 16, which agrees with that used for analysis of the thermoelectric-power data for $PtGa_2$.[9] We should point out that the detailed charge transfer in $PtGa_2$ is different from that in $AuAl_2$. From both the theoretical calculation[41] and the XANES data,[42] we notice that in $AuAl_2$, although the total charge transfer is also from the transition metal (Au) to a metalloid (Al), the larger Au-site s and d charge loss is partially compensated by the smaller gain in the Au-site p and f charges.

C. EXAFS spectra and bonding parameters

Figures 7(a) and 7(b) show the experimental (solid lines) and theoretical fitted (open circles) Fourier transforms of the k^3-weighted Pt L_3- and Ga K-edge EXAFS spectra for $PtGa_2$, respectively, while Fig. 7(c) shows those spectra for Pt foil. The bond distance R, the coordination number N, and

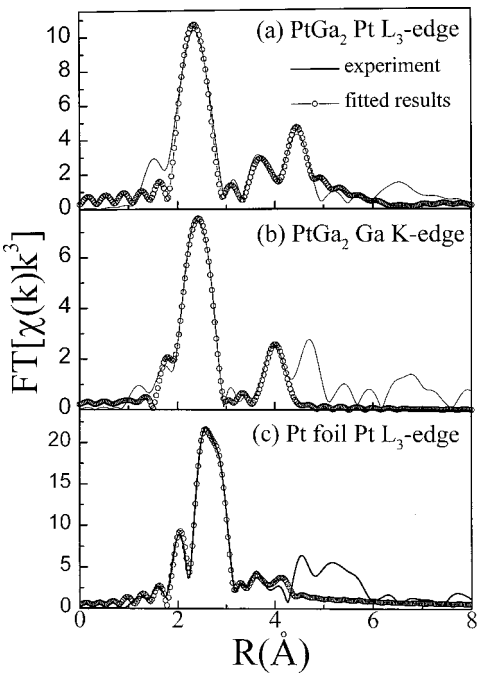

FIG. 7. The experimental (solid lines) and theoretical fitted (open circles) Fourier transforms of k^3-weighted (a) Pt L_3-edge EXAFS spectra for $PtGa_2$, (b) Ga K-edge EXAFS spectra for $PtGa_2$, and (c) Pt L_3-edge EXAFS spectra for Pt foil.

the scaling constant σ^2, for the first shell around the Pt or Ga atom for Pt foil and for $PtGa_2$ derived from the Pt L_3- or Ga K-edge EXAFS spectra are listed in the third, fourth, and fifth columns, respectively, in Table IV. The Pt-Pt bond length for Pt foil is 2.77 Å, which is exactly the same as the bulk value. The Pt-Ga and Ga-Pt bond lengths for $PtGa_2$ are 2.58 and 2.55 Å, respectively, which are essentially the same as the bulk value of 2.56 Å; while the Pt-Pt and Ga-Ga bond lengths for $PtGa_2$ are 4.23 and 2.83 Å, respectively, which are very close to the respective bulk values of 4.18 and 2.96 Å. However, the agreement between the N values and those expected from simple crystal-structure calculation is much worse. For example, in $PtGa_2$ the Pt atom has eight nearest-neighbor Ga atoms, and 12 second-nearest-neighbor Pt atoms; while the Ga atom has four nearest-neighbor Pt atoms, and six second-nearest-neighbor Ga atoms. The corresponding values obtained from the EXAFS analysis are 3.4, 15.6, 2.5, and 3.9. This is because the N values contain much more uncertainty than the R values in the EXAFS analysis, and also because the $PtGa_2$ sample contains some magnetic impurities and defects.[9]

TABLE IV. The bond distance (R), the coordination number (N), and the scaling constant (σ^2) for the first shell around the Pt or Ga atom for Pt foil and for $PtGa_2$ derived from the Pt L_3- or Ga K-edge EXAFS spectra.

Edge (Material)	Shell	R (Å)	N	σ^2 (10^{-3} Å^2)
Pt L_3 (Pt foil)	Pt-Pt	2.77	13.6	6.1
Pt L_3 ($PtGa_2$)	Pt-Ga	2.58	3.4	4.8
	Pt-Pt	4.23	15.6	10.2
Ga K ($PtGa_2$)	Ga-Pt	2.55	2.5	7.9
	Ga-Ga	2.83	3.9	10.1

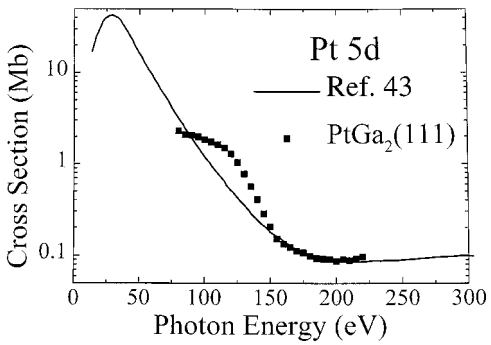

FIG. 8. Photon-energy dependence of the Pt 5d band intensity for the (111) face of $PtGa_2$. The solid line is the atomic cross section calculated by Yeh and Lindau (Ref. 43) of the Pt 5d states for elemental Pt.

D. Photon-energy dependence of the Pt 5d bands

The photon-energy dependence of the Pt 5d band intensity for $PtGa_2$ in the range $80 \leqslant h\nu \leqslant 220$ eV is shown in Fig. 8 as filled squares. Also shown in Fig. 8 as a solid line is the atomic cross section of the Pt 5d states calculated by Yeh and Lindau[43] for elemental Pt. The data points were obtained by correcting the photoemission spectra for a Shirley-type inelastic background,[44] measuring the area under the photoemission energy distribution curve in the range $2 \leqslant E_B \leqslant 6.5$ eV, and correcting this area with respect to the incident photon flux. They were then normalized to the atomic cross-section value at $h\nu = 200$ eV, where the atomic cross section shows a Cooper minimum.[45] The bump in the experimental data for $h\nu = 100-140$ eV is caused by non-d-weight bands dispersing outside the energy window 2–6.5 eV for area integration. That is, the sharp peak at $E_B = 5.5$ eV in Fig. 2 exists precisely in this range of 100–140 eV, which corresponds to the top of the lower Pt 5d band. This lower 5d band disperses to below 7 eV along Γ-L and mixes more with the s-p bands than do the other two 5d bands (the present FLAPW calculation shows that the Pt d weight for $PtGa_2$ is 96%, 43%, and 48% at the Γ_8^1, Γ_7, and Γ_8^2 points, respectively). We note that in this photon-energy range, the Pt 5d states of $PtGa_2$ show atomiclike behavior, which is in sharp contrast to the solid-state effect observed for the Pt 5d states in Pt metal.[46]

IV. CONCLUSIONS

Synchrotron-radiation-excited angle-resolved photoemission and XAS spectra for the (111) face of $PtGa_2$ are presented. The band structure and DOS for $PtGa_2$ are also calculated with the FLAPW method. The experimental and theoretical bands and the XANES spectra and the DOS curves for $PtGa_2$ show generally good agreement. The binding energies at Γ_8^1, Γ_7, and Γ_8^2 for $PtGa_2$ are within 8% of the corresponding values for Au, suggesting that these two materials have very similar electronic structures. Charge

transfers from Pt to Ga in forming the $PtGa_2$ compound. EXAFS spectra of $PtGa_2$ are analyzed to yield its structural parameters. The photon-energy variation of the Pt $5d$ photoemission intensity for $PtGa_2$ shows atomiclike behavior.

ACKNOWLEDGMENTS

L.S.H. acknowledges the National Science Council (NSC), Taiwan, Republic of China for support at the Department of Physics, University of Michigan (UM), Ann Arbor, Michigan, where part of this work was performed. We thank J.-F. Lee and C.-J. Chen for their help at the SRRC wiggler beamline, and B. C. Hsu for his assistance in starting up the theoretical calculations. G.Y.G. acknowledges support from the NSC, Grant No. 89-2112-M002-0025. Work at UM was supported by the U.S. DOE (Grant No. DE-FG-02-90ER45416) and the U.S. NSF (Grant No. DMR-94-23741).

[1] J. H. Wernick, A. Menth, T. H. Geballe, G. Hull, and J. P. Maita, J. Phys. Chem. Solids **30**, 1949 (1969).
[2] L.-S. Hsu, Phys. Lett. A **184**, 476 (1994).
[3] L.-S. Hsu, H.-W. Huang, and K.-L. Tsang, J. Phys. Chem. Solids **59**, 1205 (1998).
[4] J. G. Nelson, W. J. Gignac, S. Kim, J. R. Lince, and R. S. Williams, Phys. Rev. B **31**, 3469 (1985).
[5] S. Kim, L.-S. Hsu, and R. S. Williams, Phys. Rev. B **36**, 3099 (1987).
[6] K. J. Kim, B. N. Harmon, L.-Y. Chen, and D. W. Lynch, Phys. Rev. B **42**, 8813 (1990).
[7] L.-S. Hsu and M. A. Tischler, Phys. Status Solidi B **214**, 419 (1999).
[8] L.-S. Hsu and K.-L. Tsang, Phys. Rev. B **56**, 6615 (1997).
[9] L.-S. Hsu, L.-W. Zhou, and R. S. Williams, J. Phys. Chem. Solids **54**, 913 (1993).
[10] L.-S. Hsu, Mod. Phys. Lett. B **8**, 1297 (1994), and references therein.
[11] L.-S. Hsu, J. D. Denlinger, and J. W. Allen, in *Application of Synchrotron Radiation Techniques to Materials Science IV*, edited by S. M. Mini, D. L. Perry, S. R. Stock, and L. J. Terminello, MRS Symposia Proceedings No. 524 (Materials Research Society, Pittsburgh, 1998), p. 179.
[12] R. J. Baughman, Mater. Res. Bull. **7**, 505 (1972); D. Swenson and B. Morosin, J. Alloys Compd. **243**, 173 (1996).
[13] J. H. Scofield, J. Electron Spectrosc. Relat. Phenom. **8**, 129 (1976).
[14] L.-S. Hsu, K.-L. Tsang, and S.-C. Chung, in *Applications of Synchrotron Radiation Techniques to Materials Science III*, edited by L. J. Terminello, S. M. Mini, H. Ade, and D. L. Perry, MRS Symposia Proceedings No. 437 (Materials Research Society, Pittsburgh, 1996), p. 53.
[15] L.-S. Hsu, K.-L. Tsang, and S.-C. Chung, Int. J. Mod. Phys. B **12**, 2757 (1998).
[16] L.-S. Hsu, G.-H. Gweon, and J. W. Allen, J. Phys. Chem. Solids **60**, 1627 (1999).
[17] L.-S. Hsu and R. S. Williams, J. Phys. Chem. Solids **55**, 305 (1994).
[18] L.-S. Hsu, K.-L. Tsang, and S.-C. Chung, J. Magn. Magn. Mater. **177-181**, 1031 (1998).
[19] L.-S. Hsu and R. S. Williams, Phys. Lett. A **178**, 192 (1993); L.-S. Hsu, Phys. Rev. B **52**, 10 858 (1995).
[20] L.-S. Hsu, J. Phys. Chem. Solids **59**, 651 (1998).
[21] J. G. Nelson, J. R. Lince, W. J. Gignac, and R. S. Williams, J. Vac. Sci. Technol. A **2**, 534 (1984).
[22] E. A. Stern, M. Newville, B. Ravel, and D. Haskel, Physica B **208-209**, 117 (1995).
[23] J. J. Rehr, J. M. de Leon, S. I. Zabinsky, and R. C. Alberts, J. Am. Chem. Soc. **113**, 5135 (1991).
[24] S. Kim, J. G. Nelson, and R. S. Williams, Phys. Rev. B **31**, 3460 (1985).
[25] P. Blaha, K. Schwarz, and J. Luitz, computer code WIEN97 (Vienna University of Technology, 1997). [Improved and updated UNIX version of the original copyrighted WIEN code, which was published by P. Blaha, K. Schwarz, P. Sorantin, and S. B. Trickey, Comput. Phys. Commun. **59**, 399 (1990).]
[26] S. H. Vosko, L. Wilk, and M. Nusair, Can. J. Phys. **58**, 1200 (1980).
[27] P. E. Blochl, O. Jepsen, and O. K. Andersen, Phys. Rev. B **49**, 16 223 (1994).
[28] R. O. Jones and O. Gunnarsson, Rev. Mod. Phys. **61**, 689 (1989).
[29] D. J. Singh, W. E. Pickett, and H. Krakauer, Phys. Rev. B **43**, 11 628 (1991).
[30] M. Koerling and J. Haeglund, Phys. Rev. B **45**, 13 293 (1991).
[31] J. P. Perdew, S. Burke, and M. Ernzerhof, Phys. Rev. Lett. **77**, 3865 (1996), and references therein.
[32] G. Y. Guo and H. H. Wang, Phys. Rev. B **62**, 5136 (2000).
[33] L. R. Testardi, Phys. Rev. B **1**, 4851 (1970).
[34] A. C. Switendick and A. Narath, Phys. Rev. Lett. **22**, 1423 (1969).
[35] T. Grandke, L. Ley, and M. Cardona, Phys. Rev. B **18**, 3847 (1978).
[36] H. Eckhardt, L. Fritsche, and J. Noffe, J. Phys. F: Met. Phys. **14**, 97 (1984).
[37] N. E. Christensen and B. O. Seraphin, Phys. Rev. B **4**, 3321 (1971).
[38] K. A. Mills, R. F. Davis, S. D. Kevan, G. Thornton, and D. A. Shirley, Phys. Rev. B **22**, 581 (1980).
[39] W. L. McMillan, Phys. Rev. **167**, 331 (1968).
[40] O. K. Andersen, Phys. Rev. B **12**, 3060 (1975).
[41] L.-S. Hsu, G. Y. Guo, J. D. Denlinger, and J. W. Allen, J. Phys. Chem. Solids (to be published).
[42] A. Bzowski, Y. M. Yiu, and T. K. Sham, Phys. Rev. B **51**, 9515 (1995).
[43] J.-J. Yeh and I. Lindau, At. Data Nucl. Data Tables **32**, 1 (1985).
[44] D. A. Shirley, Phys. Rev. B **5**, 4709 (1972).
[45] J. W. Cooper, Phys. Rev. Lett. **13**, 762 (1964); U. Fano and J. W. Cooper, Rev. Mod. Phys. **40**, 441 (1968).
[46] G. Rossi, I. Lindau, L. Braicovich, and I. Abbati, Phys. Rev. B **28**, 3031 (1983).